A Patient-Specific Single Equivalent Dipole Model

Gabriel Cardoso[1,4,6], Geneviève Robin[2], Andony Arrieula[3,4,5], Mark Potse[5,4,3], Michel Haïssaguerre[4,6,7], Eric Moulines[1], Rémi Dubois[4,6]

[1] CMAP, Ecole Polytechnique, UMR 7641, Palaiseau, France
[2] CNRS, LaMME, Université d'Evry Val d'Essonne, Evry, France
[3] CARMEN Research Team, Inria Bordeaux – Sud-Ouest, Talence, France
[4] IHU Liryc, fondation Bordeaux Université, Pessac, France
[5] Univ Bordeaux, IMB, UMR 5251, Talence, France
[6] Univ Bordeaux, CRCTB U4045, INSERM, Bordeaux, France
[7] Bordeaux University Hospital (CHU), Electrophysiology and Ablation Unit, Pessac, France

Abstract

Sophisticated models for the electrocardiographic inverse problem are available, but their reliance on imaging data and large numbers of electrodes limit their use. Simple models such as the single equivalent dipole model (SEDM) therefore remain relevant. We developed a probabilistic approach to the equivalent unbounded uniform single dipole problem and developed a natural extension to the bounded nonuniform case that relies on a patient-specific statistical inference of the propagation mechanism between the location of the dipole and the electrode locations. The two models were tested on data simulated with a detailed heart-torso model with four different activation sequences and three different sets of tissue characteristics. We observed a throughout enhancement of the ability to reconstruct the ECG of the patient-specific model when compared to the uniform unbounded dipole model.

1. Introduction

Modeling the electrical activity of the heart as a single, time-varying electric current dipole dates back to Einthoven et al.[1]. Einthoven's triangle [2, volume 1 section 10.3.6] assumes a single fixed dipole in an unbounded uniform body. Information from leads I, II, III of the standard ECG allows measurement of the individual components of such a dipole. However, the assumption of an uniform body significantly limits the interpretability of the resulting dipole parameters. A current dipole with magnitude $\boldsymbol{p}_t \in \mathbb{R}^3$ and position $\boldsymbol{x}_p \in \mathbb{R}^3$ in a conductor with an arbitrary bounded volume, generates a potential

$$y_t^i = \boldsymbol{c}(\boldsymbol{x}_i, \boldsymbol{x}_p) \cdot \boldsymbol{p}_t, \quad \boldsymbol{c} : \mathbb{R}^3 \times \mathbb{R}^3 \to \mathbb{R}^3 \tag{1}$$

at position $\boldsymbol{x}_i \in \mathbb{R}^3$, where $i \in \{1, ..., K\}$ is the index of the measurements [2, Chapter 10]. This is the main ground for the development of vectorcardiography and Frank's lead system, whose goal is to measure each of the components of $\boldsymbol{p}_t$ in an orthogonal basis in the equivalent electrical space. Frank [3] established a method for estimating an orthogonal lead system, by inducing a current dipole in three directions in an artificial torso and measuring the resulting potential at the surface. This led to the creation of a 3d lead system called the Frank's lead system defined by F_x, F_y, F_z leads that represents an orthogonal basis of the equivalent electrical space. The vectorcardiogram obtained using this lead system has been successfully applied to a number of problems [4].

An important limitation of this approach is that it is not patient-specific, being experimentally derived from an artificial torso. Therefore we developed a new patient-specific SEDM and a method to solve the related inverse problem (finding the posterior distribution of the latent parameters given the data of a given patient) in a Bayesian statistical setting. We tested the method on simulated ECGs produced with a detailed human heart and torso model, with different activation origins and different conduction properties.

2. Equivalent Unbounded dipole model

Our goal is to estimate the posterior distribution of the parameters given the observed data.

The following notation will be used throughout the rest of this paper: If a_t^i is a scalar variable indexed by $i \in \{1, ..., K\}$ and $t \in \{1, ..., T\}$, we write $\boldsymbol{A} = (a_1^1, a_1^2, ...a_T^K)$. We will write $\|\boldsymbol{a}\|$ for the L2-norm (Euclidean norm) of the vector $\boldsymbol{a}$. Assuming propagation through an unbounded homogeneous medium, the torso

potentials are

$$y_t^i|\boldsymbol{p}_t \sim \mathcal{N}\left(\boldsymbol{c}_{\text{HOM}}(\boldsymbol{x}_i)\cdot\boldsymbol{p}_t, \sigma_{i,t}^2\right), \boldsymbol{c}_{\text{HOM}}(\boldsymbol{x}_i) = \boldsymbol{x}_i/\|\boldsymbol{x}_i\|^3 \tag{2}$$

where p_t represents the dipole vector of a current dipole placed at $\mathbf{0}$.

If the measurements $(y_t^i)_{t=1,\dots,T}^{i=1,\dots,K}$ start at the beginning of the QRS complex of the ECG then it is reasonable to expect $\boldsymbol{p}_t$ to be small at the beginning, since it corresponds to the onset of the activation of the ventricles. There is no *a priori* reason to expect that the components of the dipole are positive or negative, so a Gaussian distribution centered on $\mathbf{0}$ is a natural candidate for the prior distribution $\boldsymbol{p}_0$.

Most of the common sampling rates in the ECG domain (sampling rate > 250 Hz) are higher than the frequency of the dipole curve $\boldsymbol{p}_t$. Therefore, we expect a small deviation between $\boldsymbol{p}_t$ and $\boldsymbol{p}_{t+1}$, i.e., we expect $\|\boldsymbol{p}_{t+1} - \boldsymbol{p}_t\|$ to be close to 0. This leads us to define the prior distribution as

$$\boldsymbol{p}_{t+1}|\boldsymbol{p}_t = \mathcal{N}(\boldsymbol{p}_t, \sigma_p^2 I), \quad \boldsymbol{p}_0 = \mathcal{N}(\mathbf{0}, I). \tag{3}$$

3. Our model

To make the SEDM model patient-specific we consider the function $\boldsymbol{c}$ as the random variable from which the posterior distribution given the observed data must be estimated for each patient. To develop a Bayesian approach, we need to define a prior over a function space and a likelihood. The main idea is to use the model developed in section 2 to define a Gaussian process as a prior distribution over a function space. For $\boldsymbol{f} : \mathbb{R}^3 \to \mathbb{R}^3$:

$$\begin{aligned} y_t^i|\boldsymbol{f}, \boldsymbol{p}_t, \boldsymbol{x}_i &\sim \mathcal{N}\left(\boldsymbol{c}_{\text{INH}}(\boldsymbol{x}_i)\cdot\boldsymbol{p}_t, \sigma_{i,t}^2\right) \\ \boldsymbol{c}_{\text{INH}}(\boldsymbol{x}_i;\boldsymbol{f}) &= \{\boldsymbol{x}_i + \boldsymbol{f}(\boldsymbol{x}_i)\}/\|\boldsymbol{x}_i\|^3 \end{aligned} \tag{4}$$

The prior over the function $\boldsymbol{f}$ will be defined as, following Bishop [5] section 6.4:

$$\boldsymbol{f} \sim \mathcal{GP}(0, k_\theta(\boldsymbol{x}, \boldsymbol{x}')) \tag{5}$$

The prior and posterior are thus determined by the choice of the kernel function k. We use a component-wise independent scaled radial basis function (RBF) kernel defined as

$$\begin{aligned} k_{\nu,l}(x, x') &= \nu \exp(-(x-x')^2/2l^2) \\ k_\theta(\boldsymbol{x}, \boldsymbol{x}') &= \text{diag}(k_{\nu_i,l_i}(\boldsymbol{x}[i], \boldsymbol{x}'[i]), i = 1, 2, 3). \end{aligned} \tag{6}$$

The parameter ν determines the scale of the covariance matrix and in our case controls the magnitude of f, i.e., how far we are from the uniform dipole model. The parameter l indicates the rate at which the covariance between two points decreases. A small l would result in more variation being allowed for f between two neighboring points x, x'.

Our goal is to obtain samples from the posterior distribution $\boldsymbol{f}(\boldsymbol{X}), \boldsymbol{P}|\boldsymbol{Y}$. Note that sampling from each conditional distribution $\boldsymbol{f}(\boldsymbol{X})|\boldsymbol{P}, \boldsymbol{Y}$ and $\boldsymbol{P}|\boldsymbol{f}(\boldsymbol{X}), \boldsymbol{Y}$ can be done by directly applying the definition of conditioning of a Gaussian process [5, Section 6.4.2] and by RTS Kalman Smoothing [6] respectively. Therefore, we can use a two-stage Gibbs sampler [7] to sample directly from the posterior by sampling sequentially from each conditional $\boldsymbol{f}(\boldsymbol{X})|\boldsymbol{P}, \boldsymbol{Y}$ and $\boldsymbol{P}|\boldsymbol{f}(\boldsymbol{X}), \boldsymbol{Y}$.

4. Numerical Evaluation

In our simulations, we considered $v = 10^{-4}$ and $l = 1$. For each configuration we discard the first 300 samples of the Gibbs sampler (the so called burn-in period) and use the following 1000 samples. We use the samples to calculate the mean posterior of each of the parameters $\boldsymbol{P}$ and $\boldsymbol{f}(\boldsymbol{X})$. The sames samples are used with eq. (2) to generate samples of the reconstructed posterior ECG measurements. The metric used to evaluate goodness of fit was the coefficient of determination, known as R^2, defined as $R^2(\boldsymbol{y}, \boldsymbol{z}) = 1 - \frac{\sum_{t=1}^T (y_t - z_t)^2}{\sum_{t=1}^T (y_t - \bar{y})^2}$ where $\bar{y} = \frac{1}{T}\sum_{t=1}^T y_t$.

We used a detailed anatomical model of the heart and torso created from computed tomography data. Simulations were performed on a bi-ventricular mesh with a uniform edge length of 200 µm. A human ventricular ionic model [8] was used with a monodomain reaction-diffusion equation. The potentials at 252 electrode locations on the torso were computed using lead fields [9]. Three anatomical configurations were created: one with a full healthy tissue, and two with low-conductivity zones with radii of 12 and 18 mm. In these zones the conductivity was 10 times smaller than in the healthy tissue. For each configuration, 3 paced beats from different origins (A, B, C) and one normal ventricular beat were simulated. The pacing locations and the low-conductivity zones are shown in Fig. 2. In total, 12 sets of signals were simulated. For computational efficiency, the signals were sampled at 500 Hz.

We placed the dipole at the barycenter of the three stimulation points A, B, and C. We use the following notation for the figures: INH-DIP (Inhomogeneous-Dipole) corresponds to the statistical model defined by eqs. (3) to (5), and HOM-DIP corresponds to the statistical model defined by eqs. (2) and (3).

We consider for each configuration (consisting of a couple of low-conduction radius and pacing type) the per patient inter-electrode median $R2$ score in section 4, where we see that the INH-DIP model performed considerably better than the HOM-DIP model. The corresponding reconstructed electrograms are shown in figure 1.

In fig. 3, we show three different posterior mean dipole curves ($\boldsymbol{p}_t$ for $t = 1, ..., T$) obtained for the sinusal rhythm but with different structural configurations (scar radii from

Stim	Scar radius	INH-DIPP	HOM-DIP
SINUSAL	0	0.897	0.670
A	0	0.918	0.386
B	0	0.822	0.265
C	0	0.840	0.344
SINUSAL	12	0.884	0.654
A	12	0.922	0.388
B	12	0.827	0.290
C	12	0.853	0.441
SINUSAL	18	0.889	0.666
A	18	0.927	0.410
B	18	0.840	0.288
C	18	0.894	0.613

Table 1. Table showing results of the inter electrode median R^2 score for each simulation setting.

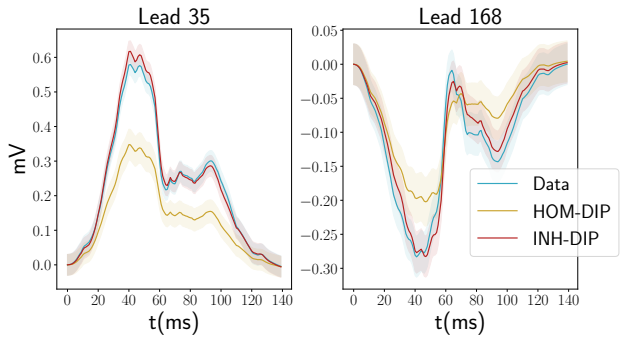

Figure 1. The means of the posterior measurements $Y|\boldsymbol{P}, X$ for each model as well as the confidence intervals (shaded) corresponding to $\mu \pm 3\sigma$ for two leads for the sinusal-18mm radius simulation.

0 to 18mm). We observe that the curves match during most of the time but are different in the end of each curve. In fig. 4, we show the mean posterior dipole curve for the sinusal rhythm with 18mm scar radius. We can see that the deviation observed in fig. 3 corresponds to the time the wave front encounters the scar region, indicating that indeed the deviations in fig. 3 indicates the inherent structural configuration.

5. Discussion

The model developed in section 2 is simplistic and several approaches have been developed to reduce the model error, e.g. by Frank [3]. However, to the best of our knowledge, none of them is based on probabilistic modeling of the function $\boldsymbol{c}$ in (1). We have presented a probabilistic framework for solving the SEDM problem that allows us to derive a natural extension to a patient-specific model that

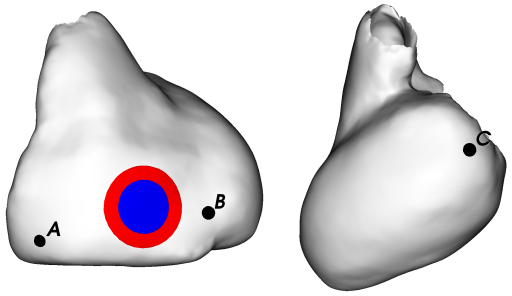

Figure 2. Mesh of the modeled heart used for simulations, with the location of the pacing sites (A, B, C) and the low-conduction zone with a radius of 12 mm in blue and a radius of 18 mm in red.

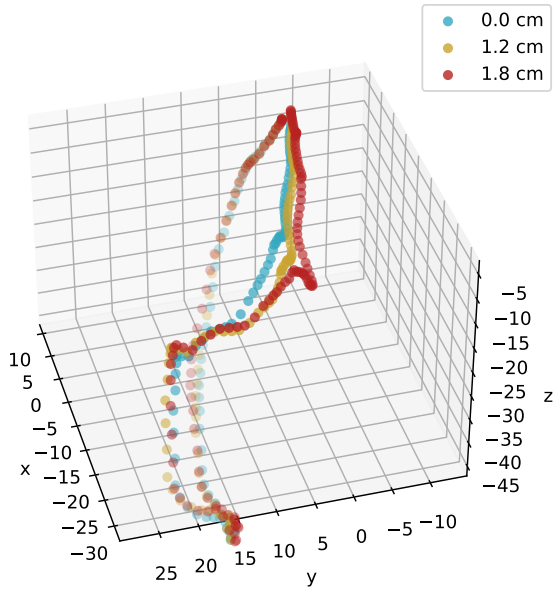

Figure 3. Illustration of the posterior mean dipole curve $\boldsymbol{p}_t$ for the sinusal rhythm with three different scar sizes, represented by the different colors.

outperforms the equivalent unbounded dipole model in all situations tested. There are several ways to further develop and validate this model. One of them is the development of the kernel function, for example, to handle the correlation between the different components of the function f. Validation with clinical data is also a major challenge, as is the ability of the model to handle even more uncertain data (no knowledge of heart placement, varying geometries).

Acknowledgements

This work was supported by the Région Nouvelle-Aquitaine, grant nr. 2017 – 1R50109 – 00013434; the European Research Council (H2020 grant agreement number

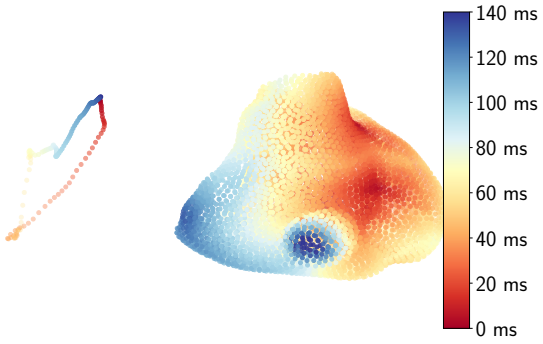

Figure 4. Illustration of the dipole curve colored (left) by the activation times, also shown in the heart surface (right) for the sinusal 18mm scar radius.

715093, ECSTATIC); and the French National Research Agency, grant references ANR-10-IAHU04-LIRYC and ANR-11-EQPX-0030. This work was granted access to the HPC resources of CINES under the allocation 2021-A0110307379 made by GENCI.

References

[1] Einthoven W, Fahr G, de Waart A. On the direction and manifest size of the variations of potential in the human heart and on the influence of the position of the heart on the form of the electrocardiogram. American Heart Journal 1950;40(2):163–211. ISSN 0002-8703. URL https://www.sciencedirect.com/science/article/pii/0002870350901657.

[2] Comprehensive electrocardiology, 2010. URL http://dx.doi.org/10.1007/978-1-84882-046-3.

[3] Frank E. An accurate, clinically practical system for spatial vectorcardiography, May 1956. URL http://dx.doi.org/10.1161/01.CIR.13.5.737.

[4] Armoundas A, Feldman A, Mukkamala R, Cohen R. A single equivalent moving dipole model: An efficient approach for localizing sites of origin of ventricular electrical activation. Annals of biomedical engineering 06 2003;31:564–76.

[5] M. C. Pattern Recognition and Machine Learning. Springer, 2016. ISBN 9780387310732.

[6] RAUCH HE, TUNG F, STRIEBEL CT. Maximum likelihood estimates of linear dynamic systems. AIAA Journal 1965;3(8):1445–1450. URL https://doi.org/10.2514/3.3166.

[7] Casella G, George EI. Explaining the gibbs sampler. The American Statistician 1992;46(3):167–174. ISSN 00031305. URL http://www.jstor.org/stable/2685208.

[8] ten Tusscher KHWJ, Noble D, Noble PJ, Panfilov AV. A model for human ventricular tissue. American Journal of Physiology Heart and Circulatory Physiology 2004; 286(4):H1573–H1589. URL https://doi.org/10.1152/ajpheart.00794.2003. PMID: 14656705.

[9] Potse M. Scalable and accurate ECG simulation for reaction-diffusion models of the human heart. Front Physiol 2018; 9:370.

Address for Correspondence

For anything related to this article, please contact the authors at Centre Hospitalier Xavier Arnozan, IHU-Liryc, Av. du Haut Lévêque, 33600 Pessac, France.